EUROPHYSICS LETTERS 1 September 1999

Europhys. Lett., **47** (5), pp. 601-607 (1999)

Electron backscattering on single-wall carbon nanotubes observed by scanning tunneling microscopy

W. Clauss(*), D. J. Bergeron, M. Freitag, C. L. Kane
E. J. Mele and A. T. Johnson

Department of Physics and Astronomy, University of Pennsylvania
Philadelphia, Pennsylvania 19104, USA

(received 23 March 1999; accepted in final form 5 July 1999)

PACS. 72.80Rj – Fullerenes and related materials.
PACS. 73.40Gk – Tunneling.
PACS. 61.16Ch – Scanning probe microscopy: scanning tunneling, atomic force, scanning optical, magnetic force, etc.

Abstract. – Single-wall carbon nanotubes, seamless cylindrical molecules formed from a graphene sheet, are either conducting or semiconducting, depending on the particular "wrapping vector" that defines the waist of the tube. Scanning tunneling microscopy experiments have tested this idea by simultaneously measuring a tube's lattice structure and electronic properties. Here we present a series of STM images of single-wall carbon nanotubes with a strikingly rich set of superstructures. The observed patterns can be understood as due to interference between propagating electron waves that are reflected from defects on the tube walls and ends, or as intrinsic to states propagating on semiconducting tubes. The measured broken symmetries can be used to directly probe electronic backscattering on the tube and provide a key element in the understanding of low-energy electron transport on these structures.

Introduction. – Single-wall carbon nanotubes (SWNTs) [1-3] are thought to be almost ideal one-dimensional quantum systems. This property is a direct consequence of the formation of a cylinder from a perfect two-dimensional "graphene" sheet. Such sheets can also pack in a well-ordered ABAB stacking sequence to form highly ordered pyrolytic graphite (HOPG). Scanning tunneling microscopy (STM) studies of the surface of this layered crystal [4] find that the low-energy band structure determines the observed contrast, rather than the atomic configuration alone. In particular, the collapse of the Fermi surface into six "K" points at the Brillouin zone edge [5] results in STM images where only the periodicity of the two-atom unit cell is seen [6]. If the few available electronic states around the Fermi energy E_F are distorted by elastic scattering at defect sites, the STM contrast can change locally to more complex patterns with larger but commensurate wavelengths [7, 8]. By wrapping a graphene sheet into a one-dimensional quantum cylinder, the general shape of the electronic bandstructure

(*) Permanent address: Institute of Applied Physics, University of Tuebingen, Germany. E-mail: wilfried.clauss@uni-tuebingen.de

© EDP Sciences

is affected only weakly. However, this introduces an additional perodic boundary condition that further reduces the number of available wave vectors around E_F, and the tube becomes metallic or semiconducting depending on the orientation of the wrapping vector [1]. Strong evidence for this picture was obtained by simultaneously measuring a tube's lattice structure and electronic properties using scanning tunneling spectroscopy [9,10]. Because of the reduced dimensionality, the spatial electron distribution on a SWNT near a defect should show even stronger deviations from the simple atomic lattice than HOPG. It is just this effect that we explore in the experiments described here.

We present here a series of STM images of single-wall carbon nanotubes with a strikingly rich set of superstructures that break the symmetry of the honeycomb lattice. Many of the observed patterns can be understood as due to interference between propagating electron waves that are reflected from defects on the tube walls and ends, or as intrinsic to states propagating on semiconducting tubes. We stress that STM and transport experiments conducted in our lab and elsewhere support the idea that individual nanotubes are atomically perfect over micron lengths. However, chemical impurities and tube ends can act as strong electron scatterers, particularly in bundles of unpurified material, as measured here. Because the spatial electron distribution results from the superposition of a small number of coherent states, the interpretation of the STM image contrast is not only of fundamental importance for the understanding of the imaging mechanism. Additionally, similar images of the scattered electron distribution give information about the nature of the scattering that also ultimately determines the SWNT transport characteristics. This is extremely important with respect to possible future applications as nano-electronic devices. The samples for the STM experiments were prepared by various methods (spin-coating, pressing, and electrodeposition) of laser-ablated nanotube material provided by the Smalley group (Rice University) [11]. Most data were obtained in high vacuum, but atomic resolution was also reliably obtained at ambient pressure. All experiments were performed at room temperature with commercial PtIr tips. Tunneling voltages used were in the range of 200–500 mV, setpoint current values were typically 200 pA. In order to strengthen the contrast of the relevant image components at high spatial frequencies, for figs. 2-4 an imaging mode was chosen with a large feedback time constant compared to the scan speed. As a consequence, the tip only followed the overall tube shape but not the atomic scale modulations. The displayed error signal in this quasi-constant-height mode can be directly interpreted as an image of the spatial electron distribution.

Figure 1 shows an STM image displaying the rich family of structures we find for single-wall tubes packed into bundles or "ropes" [11,12]. In the scan we see a bundle of parallel tubes lying on an atomically flat gold surface. Since all tubes share the same honeycomb lattice structure, the variations we observe from tube to tube in a bundle are not explained by structural variations, but can be understood in the unified framework of electron scattering we outline below. The first common motif is the presence of a peaked electron density along chains of bonds that spiral around the tube wall. Second, many images show modulations with a period larger than, but commensurate with, the underlying lattice. This is seen in regions A and C in fig. 1, where the fundamental cell in region C is three times larger in area than in region A. Third, there are tubes where the lattice periodicity or orientation changes abruptly (region B), as well as tubes whose image is "noisy", with no well-defined lattice structure (*e.g.*, the central tube running diagonally through fig. 1). It is known that asymmetries in the STM tip can produce distortions in images of graphite [13]. All the different features of fig. 1, however, are obtained with the *same* tip during a *single* scan, making it very unlikely that they are tip artifacts. Moreover, the superstructures seen here are qualitatively reproduced in dozens of images taken with a variety of tips and nanotube samples over several months.

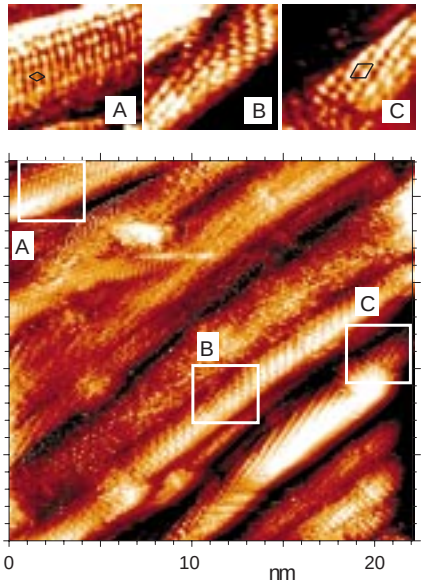

Fig. 1

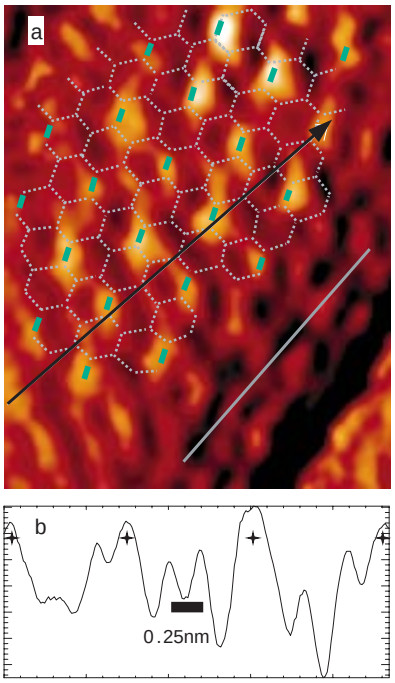

Fig. 2

Fig. 1. – Large-scale scan of a bundle with tubes of various diameters and chiralities. The upper panels are enlarged regions of tubes with different image symmetries (see text).

Fig. 2. – a) High-resolution image of a tube surface with a superposition of the primitive honeycomb lattice and a $\sqrt{3} \times \sqrt{3}R30^\circ$ superstructure of enhanced bonds along the tube marked by green bars. The atomic lattice is shown in light grey; some image distortion occurs due to tube curvature. The black line along the zig-zag direction, at an angle of 12° to the tube axis, is the scan direction for b). The orientation of the tube axis is marked by the line in the lower right corner. b) Scan along the black line indicated in a). Peaks occur at 0.25 nm intervals, as expected for the graphite lattice, but every third peak (marked by a star) is enhanced due to the $\sqrt{3} \times \sqrt{3}$ superstructure.

Figure 2 is an STM image where both translational and rotational symmetry are broken. As indicated by the gray lines and green bars, alternate bonds that run along the armchair direction of the tube have enhanced electron density. This appears clearly in the line scan of fig. 2(b), where we see peaks separated by 0.25 nm, the expected period of the graphite lattice. However, every third peak is more intense than the others, consistent with a well-defined $\sqrt{3} \times \sqrt{3}R30^\circ$ superlattice. This superlattice is very common in our images and can be seen several times in fig. 1.

In fig. 3 we show how the superstructure symmetry and period can change abruptly on a *single* tube. Starting in the image's lower left corner and moving towards the center, there is a "striped" spiral pattern with the period of the graphite lattice that merges with a tube segment with a clear $\sqrt{3} \times \sqrt{3}$ superstructure. The $\sqrt{3} \times \sqrt{3}$ area contacts an irregular region where the image is strongly disturbed. As described below, we interpret this disordered region as a chemical or other impurity responsible for strong electron wave scattering. By measuring the misalignment between the tube axis and a primitive translation vector, we assign the tube a chiral angle of 13° with respect to the armchair direction.

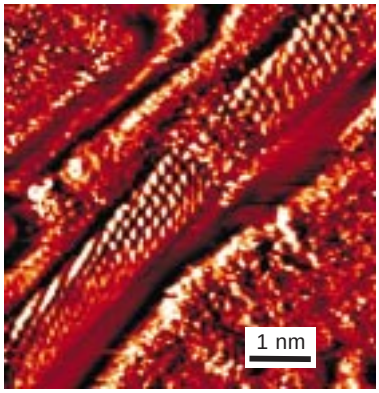

Fig. 3. – An image with a severely disordered, 2 nm long region that appears to be the source of a $\sqrt{3} \times \sqrt{3}$ electronic superstructure. With increasing distance from the defect, the superstructure continuously evolves into the primitive lattice. The two tube segments on each side of the defect form an angle of 6°. The lattice orientation is identical on both sides of the disordered region, suggesting that the defect is a chemical impurity and *not* a structural defect that changes the tube wrapping vector.

In some cases the asymmetry in the STM image depends on the *sign* of the tunnel bias voltage. For example, fig. 4 presents two images of the same tube acquired simultaneously with opposite bias voltage polarities in the forward and backward scans. Each image has a "striped" broken symmetry, but the chirality of the spiral chain reverses when the bias polarity is inverted, rotating the stripes through 60°. We observe this change in the image chirality *only* if we invert the bias voltage during the reverse scan, implying that this effect is due to the change in bias voltage, not scan direction. The appearance of two rotated versions of the striped pattern excludes the possibility of tube torsion or an image artifact produced by an asymmetric tip. However, as discussed below, such an image reversal is a signature of tunneling into or out of a semiconducting tube.

We propose that the asymmetries observed in these experiments are *interference patterns* that are sensitive to coherence between electronic states propagating "forward" and "backward" along a tube [7]. For a perfect graphene sheet, or a sheet rolled into a defect-free conducting nanotube, the electron eigenstates are simple plane waves. Tunneling experiments

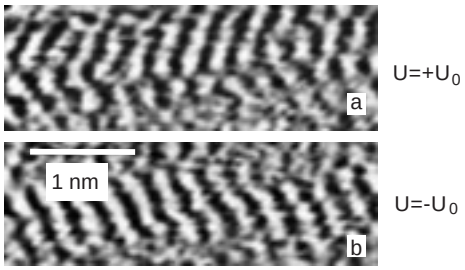

Fig. 4. – Atomic resolution images of a single tube taken with opposite voltage polarities. The images show striped spiral patterns rotated by 60° with respect to each other. Careful analysis of the superposition of the images shows that the zig-zag direction is at an angle of 5° to the tube axis.

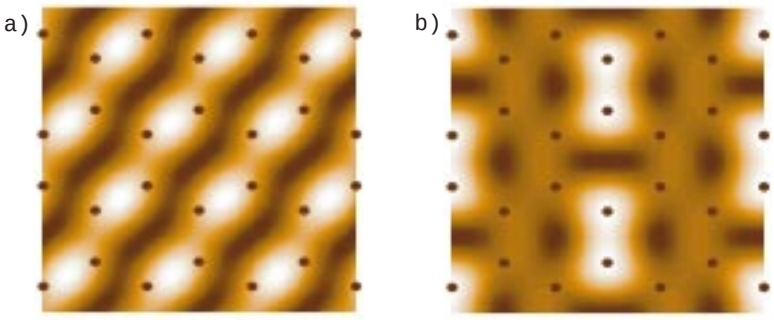

Fig. 5. – Simulated STM images of an armchair tube with scattering between electron eigenstates. a) Scattering without change in momentum produces a chiral pattern in the electron density. b) Scattering between the two Fermi points K and K′ produces a $\sqrt{3} \times \sqrt{3}$ superstructure.

probe states near the K and K′ points at the Brillouin zone corners. In contrast to a conventional metal, each of the Fermi points has both a forward and backward propagating branch of electron eigenstates, so the low-energy states can be represented using four plane waves ψ_α, where α is a four-component index describing two momenta and two branches. For *perfect* tubes the charge density of each plane wave has the full periodicity and symmetry of the graphite plane. However, chemical impurities, tube defects and ends reflect the incident plane-wave states, so the electron eigenstates contain a coherent superposition of the basis states ψ_α. For electrons on a finite tube segment, scattering from both ends gives the tube a spectrum of perfect standing waves whose charge density can break both the translational and rotational symmetries of the graphene sheet [14]. For scattering from defects on tube walls, the incident wave is partially reflected. This produces off-diagonal correlations in the density matrix $\rho_{\alpha\beta} = \langle \psi_\alpha^\dagger \delta(E - \mathcal{H}) \psi_\beta \rangle$ that determine the observed image symmetries. There are three generic features of this backscattering, all of which are observed in the images in figs. 1-4.

a) Because each Fermi point (K and K′) contains both a forward and backward moving branch of electronic states, we can have backscattering with no change in momentum. Physically, this means that the charge density in the electronic standing wave retains the lattice translational symmetry but *breaks* its rotational symmetry. The most striking situation occurs when the reflection amplitude between the branches has an imaginary part. This leads to a chiral density wave with charge density maxima along a bond chain that spirals around the tube. Figure 5(a) shows the effect on the local density of states calculated for an armchair tube with a [10,10] wrapping vector. We find that a reflection amplitude of this symmetry can be produced by any defect that breaks the symmetry between the two sublattices of the graphene sheet. The appearance of these structures does not imply that the tube is under torsion; indeed fig. 5(a) is calculated for a strain-free (untwisted) armchair tube.

b) Backscattering between plane-wave states at K and K′ produces a tunneling image that breaks the *translational* symmetry of the graphene sheet. Large momentum backscattering produces a $\sqrt{3} \times \sqrt{3}$ modulation of the tunneling image, an effect reminiscent of Friedel oscillations in solids, where forward and backward scattered waves with wave vectors $\pm k_{\mathrm{F}}$ combine to yield an oscillation at their difference of $2k_{\mathrm{F}}$. Two inequivalent amplitudes r_a and r_b describe backscattering with a positive or negative change of momentum. In fig. 5(b) we show the results for an armchair tube with perfect backscattering from a "hard" wall, $r_a = r_b = 1$. We observe a $\sqrt{3} \times \sqrt{3}$ pattern where the electron density is peaked in one third

of the tube's azimuthal bonds. In fig. 3 we observe exactly this pattern in the experiment, and the region with the $\sqrt{3} \times \sqrt{3}$ modulation contacts a disordered area that we interpret as a strong scatterer.

The two phenomena described above will be affected by energy averaging due to the finite STM tip bias voltage V. In the simplest picture, the measured electron density is the sum of a set of scattered waves up to energy eV whose wave vector varies linearly with electron energy due to the unusual band structure of metallic nanotubes. This implies that the electron density oscillations will slowly be reduced in amplitude on a length scale given by hv_{F}/eV, where $v_{\mathrm{F}} = 8.1 \times 10^5$ m/s is the Fermi velocity (taken to be that of graphite). This gives a decay length of order 5-10 nm, or more than 20 unit cells. This is in qualitiative agreement with transitions between STM image textures seen in figs. 1 and 3. We stress that this model of energy averaging could be modified by many effects (*e.g.*, multiple scattering due to a high impurity density), and verifying the application of this picture to experiment remains the subject of future work.

c) Semiconducting tubes have a gap in their energy spectrum; exactly at the band edges one has a standing wave with an equal mixture of forward and backward propagating plane waves. Here the backscattering is not due to a defect, but instead occurs because the unperturbed plane waves do not satisfy periodic boundary conditions around the tube waist, so waves need to be combined in pairs to match smoothly around the tube. The charge densities of the resulting states preserve the lattice translational symmetry, but break its sixfold rotational symmetry. The symmetry-breaking at the conduction and valence band edges is *complementary*; a superposition of the two charge densities has the full sixfold graphene symmetry that is broken in each image separately. Although the precise image structure depends on the chiral angle, we find that for tubes with near-armchair wrapping, STM images at the two band edges exhibit complementary spiral stripes whose helicity reverses when the bias voltage is reversed. Figure 4 shows precisely this striking signature of a semiconducting tube. A more detailed discussion of the effect of tunnel bias and chiral angle on tube STM images is reported elsewhere [15].

In conclusion, the rich and complex structure observed in the experimental images has a single, simple physical interpretation. These images present a real-space picture of electron wave scattering from tube boundaries and defects. The sensitivity of electronic states to such structural perturbations is a fundamental phenomenon characteristic of all mesoscopic systems, and carbon nanotubes provide a unique opportunity to explore these effects in quantitative detail.

***

This research was supported by grants from the U.S. NSF (grant number DMR98-02560), Deutsche Forschungsgemeinschaft (WC), David and Lucile Packard Foundation (ATJ), and the LRSM, a Materials Science and Engineering Center Program of NSF under award DMR96-32598 (DJB). We thank J. E. Fischer for useful discussions.

REFERENCES

[1] Hamada N., Sawada S. and Oshiyama A., *Phys. Rev. Lett.*, **68** (1992) 1579.
[2] Mintmire J. W., Dunlap B. I. and White C. T., *Phys. Rev. Lett.*, **68** (1992) 631.
[3] Saito R., Dresselhaus G. and Dresselhaus M. S., *Appl. Phys. Lett.*, **60** (1992) 2204.
[4] Wiesendanger R., *Scanning Probe Microscopy and Spectroscopy* (Cambridge) 1994.
[5] Dresselhaus M. S., Dresselhaus G. and Eklund P. C., *Science of Fullerenes and Carbon Nanotubes* (San Diego) 1996.

[6] R. WIESENDANGER and D. ANSELMETTI, in *Surface Properties of Layered Structures*, edited by G. BENEDEK (Amsterdam) 1992.

[7] MIZES H. A. *et al.*, *Science*, **244** (1989) 599.

[8] YAN J. *et al.*, *J. Appl. Phys.*, **75** (1994) 1390.

[9] WILDÖER J. W. G., VENEMA L. C., RINZLER A. G., SMALLEY R. E. and DEKKER C., *Nature*, **391** (1998) 59.

[10] ODOM T. W., HUANG J. L., KIM P. and LIEBER C. M., *Nature*, **391** (1998) 62.

[11] THESS A. *et al.*, *Science*, **273** (1996) 483.

[12] CLAUSS W., BERGERON D. J. and JOHNSON A. T., *Phys. Rev. B*, **58** (1998) R4266. *Jpn. J. Appl. Phys.*, **37** (1998) 3809.

[13] MIZES H. A., PARK S. and HARRISON W. A., *Phys. Rev. B*, **36** (1987) 4491.

[14] Experimental evidence for this effect has recently been reported by L. C. VENEMA *et al.*, *Imaging electron wave functions of quantized energy levels in carbon nanotubes*, *Science*, **283** (1999) 52.

[15] KANE C. L. and MELE E. J., to be published in *Phys. Rev. B*, Rapid Communications.